3D GEO-REFERNECING OF FREE MODEL THROUGH 3D-TO-2D ALIGNMENTS AT THE CE-5 LANDING SITE

Yuan Li*

School of Geospatial Engineering and Science, Sun Yat-Sen University, Zhuhai, Guangdong, China
(liyuan226@mail.sysu.edu.cn)

Commission II, WG II/1

KEY WORDS: 3D geo-referencing, CE-5 landing site, Descent images, DEM, DOM.

ABSTRACT:

The descent camera mounted on the CE-5 lander captured abundant images during the landing, which can be used to generate local terrain models with details from sub-meter to millimetre scales. But unlike Earth, high-precision control data are unavailable on the Moon especially for small regions like the landing sites, making it hard to define exact geo-reference of the local terrain models, which is essential for topographic and geomorphological mapping and analyses. To tackle this problem, this paper proposes a method for geo-referencing free 3D models generated from the CE-5 descent images based on low-resolution geo-referenced orbiter data. On account to the large discrepancy between the accuracies in the horizontal and vertical directions of orbiter data, the proposed method used two independent alignments in 3D and 2D spaces respectively to reduce the impacts of accuracy unevenness of the reference data. The 3D alignment is performed based on mass features to align the base-plane of the free model, and the 2D alignment is performed based on matched point features projected on the base-plane to define the scale and orientation of the model. After these the alignments, the free model is ultimately enriched with geo-reference information and used to generate fine-scale DEM and DOM of the CE-5 landing site. The average horizontal distance between the referenced data and the geo-referenced data is 2.19 m with a small standard deviation of 1.48 m, and the average height difference between the generated DEM and the reference DEM is 2.78 m, indicating a reliable 3D geo-referencing result.

1. INTRODUCTION

3D geo-referencing for digital elevation model (DEM) and digital orthoimage (DOM) is compulsory for globally planetary spatial analyses, but it can also be essential for locally fine-scale topographic and geo-morphologic mapping when it is regarded to e.g. slope, aspect and surface roughness analyses (Guo et al., 2021; Wu et al., 2021). Generally, the DEM and DOM are generated from images through photogrammetry processing, and their 3D geo-reference information can be obtained based on the known orientations of the cameras, or estimated using control data with accuracy higher than the precision of the DEM/DOM. However, for fine-scale planetary mapping, camera orientations and control data that can meet the requirements are always unavailable, and consequently only free models without geo-reference can be obtained.

The CE-5 mission was launched on 24 November 2020, landed in Northern Oceanus Procellarum of the Moon on 1 December 2020, and left the lunar surface on 3 December 2020 after collecting lunar samples. During its descending, the descent camera (DesCam) mounted on the CE-5 lander recorded a video containing 484 frames. Combining the radio-tracking, Wang et al. (2021) using these descent images localized the landing site of the CE-5 lander to be (51.92°W, 43.06°N). This localization process also produced ortho images from the descent images through affine transformation. However, these ortho images only contained horizontal geo-reference, and the affine transformation ignored the impacts of topographic reliefs, resulting in inaccuracies in the ortho images.

For 3D geospatial landing site mapping, both horizontal and vertical geo-references should be defined. A general way to produce geo-referenced 3D terrain models from images is using photogrammetric techniques based on Ground Control Points (GCPs) measured from existing DEM and DOM products (Di et al., 2020; Liu et al., 2019). While the CE-5 descent camera capturing images from kilometres to meters altitude, corresponding ground spatial resolution (GSP) of the descent image varies from sub-meter to millimetre scales. However, existing DEM/DOM products with known geo-references are mostly generated from orbiter images, which means the resolutions and accuracies of these products can be far away from meeting the requirements of geo-referencing a fine-scale 3D model. For example, the resolution of the Lunar Reconnaissance Orbiter Camera (LROC) Narrow Angle Camera (NAC) images covering the CE-5 landing site can be as high as 1 m/pixel, the resolution of SLDEM2015 is about 60 m/pixel (Barker et al., 2016), and the resolutions of the CE-2 DOM and DEM are 7 m/pixel and 20 m/pixel, respectively (Li et al., 2018). The limited accuracies of GCPs measured from such low-resolution satellite data products often lead to the failure of the photogrammetric processing.

Another strategy is firstly to generate a free model from the high-GSP images, and then align it to geo-referenced models using 3D registration methods e.g. the Iterative Closest Point (ICP) algorithm (Besl and McKay, 1992). But it is notable that the ICP and its variants are only applicable for rigid transformation by estimating six orientation parameters regarding to rotation and translation, while for aligning a free model to geo-referenced models, an additional parameter — scale — should also be determined. However, introducing the scale parameter makes the alignment easy to fall into local optimum, especially when where are huge differences between the resolutions of the resource data and the reference data, and also differences between the accuracies in horizontal and vertical directions of the reference data.

In fact, as the accuracy of the reference DEM is always considerably lower than that of the reference DOM, it is expected that the reference DEM and DOM can be used separately, so that accuracy of the 3D geo-referencing can be guaranteed as high as possible. Thus, this paper proposes a two-step method for aligning a free model generated from the CE-5 DesCam images to geo-referenced LROC NAC and CE-2 products that have different resolutions and accuracies. The first step is performed based on mass features in 3D space to align the base-plane of the free model, and the second step is performed based on point features in 2D base-plane space to determine its scale and orientation. Finally, the aligned CE-5 DesCam DOM and DEM is compared with the reference data. The result showed that the average distance between the CE-5 DesCam DOM and the reference DOM is 2.19 m, and the average height difference between the CE-5 DesCAM DEM and the reference DEM is 2.78 m.

2. 3D GEO-REFERENCING THROUGH 3D-TO-2D ALIGNMENTS

2.1 Overview of the Approach

As shown in Figure 1, firstly a free model is ***m*** generated from the CE-5 descent images using photogrammetric techniques without control data. Then the proposed approach carries out the 3D geo-referencing through two alignments in 3D and 2D spaces, respectively, based on two sets of matched 3D key points extracted from the free model and the reference data.

2.2 Pre-processing

At the pre-processing stage, source 3D key points ***p***, which are mostly the centroids of small craters or large rocks. The corresponding reference 3D key points are firstly measured from the reference LROC NAC image (1.1856 m/pixel), where their horizontal coordinates (X, Y) can be defined, and then the altitude Z values are determined by interpolating the reference CE-2 DEM (20 m/pixel) with the X-Y coordinates. The Random Sample Consensus (RANSAC) algorithm (Schnabel et al., 2007) is then performed on the reference 3D key points to fit a base-plane Π, and points with distances to Π greater than a given threshold are regarded as outliers and removed. Corresponding outliers in the source 3D key points are also removed, and the remained points in p are used to fit a source base-plane π. Figure 2 (a) shows the distribution of key points after outlier removal, it can be seen that the remained key points are mostly emplaced at flat areas with slope less than 4°. Figure 2 (b) and (c) show the fitted reference base-plane Π and the source base-plane π respectively.

Denoting the source 3D key points extracted from the free model as ***p***, for each $p \in \boldsymbol{p}$, its coordinates are (x, y, z). Denoting the reference 3D key points as ***P***, the coordinates of each point $P \in \boldsymbol{P}$ are (X, Y, Z). It is notable that the accuracies of X and Y are much higher than the accuracy of Z in ***P***. Considering this fact, the 3D alignment takes the entire set of 3D key points to fit a base-plane and orientate the base-plane using mass vector features, so that inaccuracies can be evenly distributed across the global region. Then the 2D alignment is performed by solving the orientation parameters between the source and reference 2D key points projected on the base-plane. Finally, with the orientation parameters obtained in the 3D and 2D alignments, the free model ***m*** is transformed into a geo-referenced model ***M***.

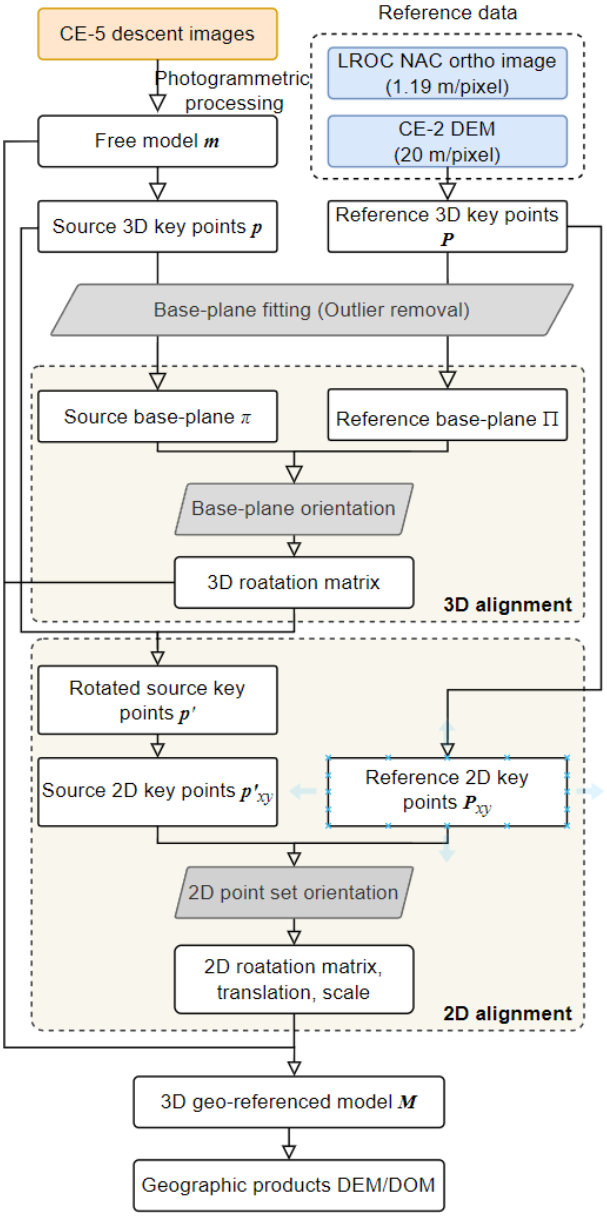

Figure 1. Workflow of the proposed approach.

2.3 3D Alignment Based-on Global Features

Denoting the number of key points in ***P*** as n, $m = C_n^2$ vectors ***V*** can be obtained from ***P***, and correspondingly, m vectors ***v*** can be obtained from ***p***. As all the normalized vectors in ***V*** form a vector mass matrix B (m × 3) and all the normalized vectors in ***v*** form a vector mass matrix A (m × 3), we can define a rotation matrix R_{3D} as in Equation (1).

$$B = A \cdot R_{3D}, \tag{1}$$

According to the Least Squares method (Björck, 1990), R_{3D} can be solved as:

$$R_{3D} = (A^T A)^{-1}(A^T B), \tag{2}$$

The source 3D key points ***p*** then can be transformed into ***p***' by Equation (3), so that ***p***' has a base-plane π' that is parallel to Π.

$$\begin{bmatrix} x' \\ y' \\ z' \end{bmatrix}^T = \begin{bmatrix} x \\ y \\ z \end{bmatrix}^T \cdot R_{3D}, \quad (3)$$

where x', y' z' are the coordinates of point in $\boldsymbol{p}'$, and x, y, z are the coordinates of point in $\boldsymbol{p}$.

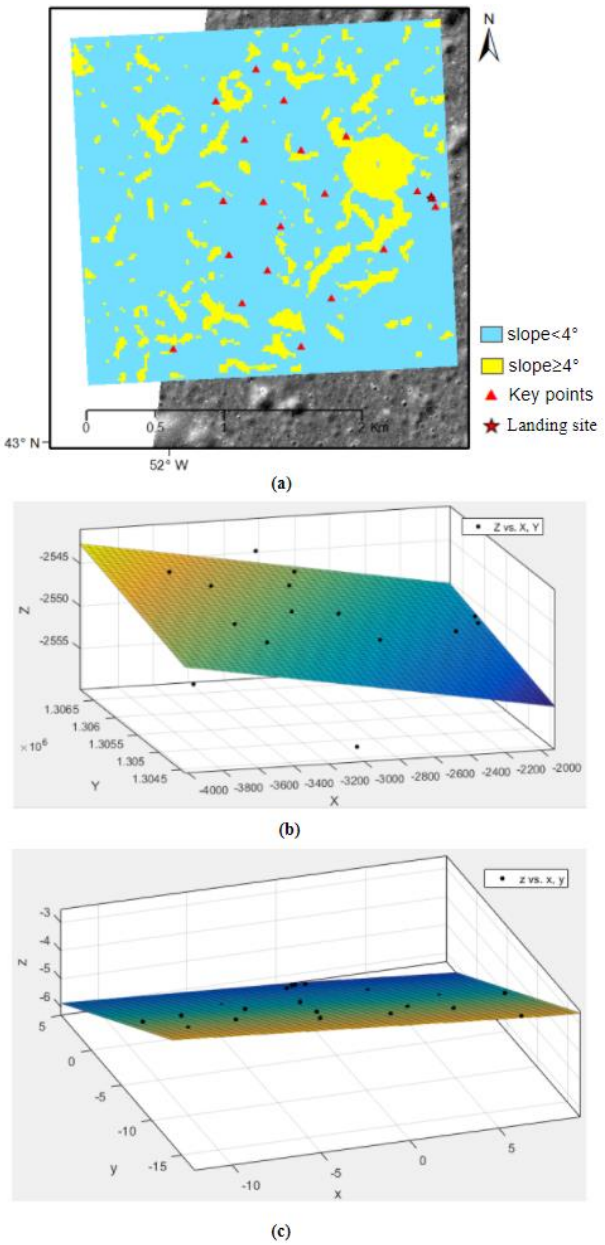

Figure 2. Base-planes estimated from the 3D key points. (a) Distribution of key points shown on the reference data, (b) reference base-plane Π estimated from the reference 3D key points, and (c) source base-plane π estimated from the source 3D key points.

In general, the purpose of R_{3D} is to rotate $\boldsymbol{p}$ as a whole to a correct orientation, where the relative altitudes of $\boldsymbol{p}$ and $\boldsymbol{P}$ are consistent (as shown in Figure 3). As the vector masses $\boldsymbol{v}$ and $\boldsymbol{V}$ are features laying in global base-planes, vertical inaccuracies of the reference data are therefore evenly distributed across the global.

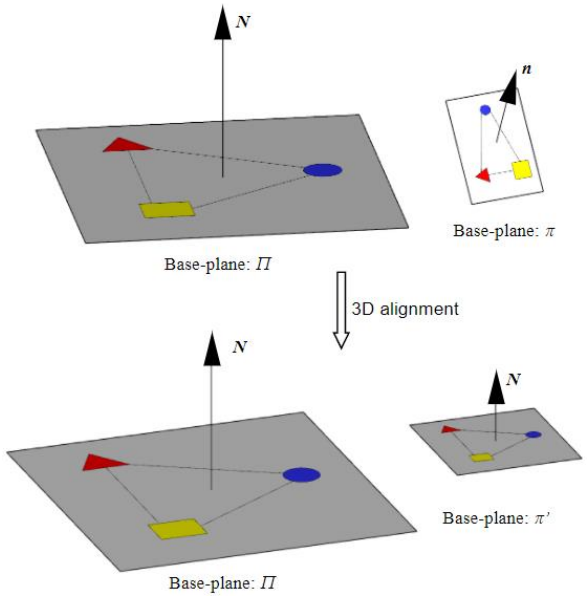

Figure 3. Demonstration of the 3D alignment of the base-planes of the source and reference data. The circle, square and triangle indicate the locations of different features.

2.4 2D Alignment Based-on Point Features

After the 3D alignment, π' is parallel to Π, but there are still transformations at the plane level as shown in Figure 3. At this stage, the transformation between $\boldsymbol{p}'$ and $\boldsymbol{P}$ is related to a scale factor s, a translation vector (T_X, T_Y, T_Z) and a rotation matrix R_{2D} for fine adjustment of rotation in X-Y plane as in Equations (4) and (5).

$$\begin{bmatrix} X \\ Y \end{bmatrix} = s \cdot R_{2D} \cdot \begin{bmatrix} x' \\ y' \end{bmatrix} + \begin{bmatrix} T_X \\ T_Y \end{bmatrix}, \quad (4)$$

$$Z = s \cdot z' + T_Z \quad (5)$$

where R_{2D} is only related to a rotation angle θ in the X-Y plane as:

$$R_{XY} = \begin{bmatrix} \cos\theta & -\sin\theta \\ \sin\theta & \cos\theta \end{bmatrix}, \quad (6)$$

According to Equations (4) and (5), the parameters s, θ and (T_X, T_Y) can be estimated only based on the horizontal data, which have much higher accuracy than the data in vertical direction. And after determining the value of s, the translation element T_Z can be easily determined as the average difference between Z and $s{\cdot}z'$ (see Equation (10)). In this way, the inaccuracies of the reference data in the vertical direction will not be introduced into the horizontal direction during solving the transformation parameters, leading to high reliability in the horizontal direction of the 3D geo-referencing. As the main purpose of this step is to determine the transformation parameters in the horizontal direction, this process is therefore called 2D alignment.

Finding the optimal solution for Equation (4) is a non-linear least squares problem and can be solved by the Gauss-newton method (Wang, 2012). As such iterative method requires good initial values as input, we defined the initial values of s, θ and (T_X, T_Y) as the follows.

$$s_0 = \mathrm{Avg}\left(\frac{\|\Delta p'_{xy}\|}{\|\Delta P_{XY}\|}\right), \tag{7}$$

$$\theta_0 = \mathrm{Avg}\left(\arctan\frac{(\Delta p'_{xy}).y}{(\Delta p'_{xy}).x} - \arctan\left(\frac{(\Delta P_{XY}).Y}{(\Delta P_{XY}).X}\right)\right), \tag{8}$$

$$\begin{bmatrix} T_{X0} \\ T_{Y0} \end{bmatrix} = \begin{bmatrix} \mathrm{Avg}(P_{XY}.\mathrm{X} - s_0 \cdot p'_{xy}.\mathrm{x}) \\ \mathrm{Avg}(P_{XY}.Y - s_0 \cdot p'_{xy}.y) \end{bmatrix}, \tag{9}$$

where s_0, θ_0 and (T_{X0}, T_{Y0}) are the initial values of s, θ and (T_X, T_Y); Avg() means the average of the values in the brackets; p'_{xy} and P_{XY} are points in $\boldsymbol{p}'$ and $\boldsymbol{P}$ projected on the horizontal plane.

After solving Equation (4), the translation element T_Z in Equation (5) can be calculated as

$$T_Z = \mathrm{Avg}(Z - s \cdot z'), \tag{10}$$

So far, all the transformation elements for the 3D geo-referencing are determined.

2.5 Generation of 3D Geo-referenced Model

After the 3D and 2D alignments, the free model $\boldsymbol{m}$ can be transformed into a model $\boldsymbol{M}$ with correct geo-reference as in the following equation.

$$\boldsymbol{M} = s \cdot \begin{bmatrix} R_{2\mathrm{D}} & 0 \\ 0 & 1 \end{bmatrix} \cdot (\boldsymbol{m}^T \cdot R_{3D})^T + \begin{bmatrix} T_X \\ T_Y \\ T_Z \end{bmatrix}, \tag{11}$$

Subsequently, geographic products, e.g. the DEM and DOM, can be generated based on $\boldsymbol{M}$ in the routine of photogrammetry (Linder, 2013).

3. EXPERIMENTAL EVALUATION

3.1 Dataset Description

3.1.1 CE-5 Descent Image Data: The descent camera onboard the CE-5 lander captured a video of about 2 minutes during the landing, totally consisting of 489 frames of images, which can available from the China's Lunar and Planetary Data Release System (https://moon.bao.ac.cn). From these images, we selected a series from frame 271 to frame 414 (see Figure 4), during which the camera kept a down-looking view and the altitude above the lunar surface is high enough from blowing the lunar dust up. The intrinsic and internal orientation parameters of the descent camera are shown in Table 1.

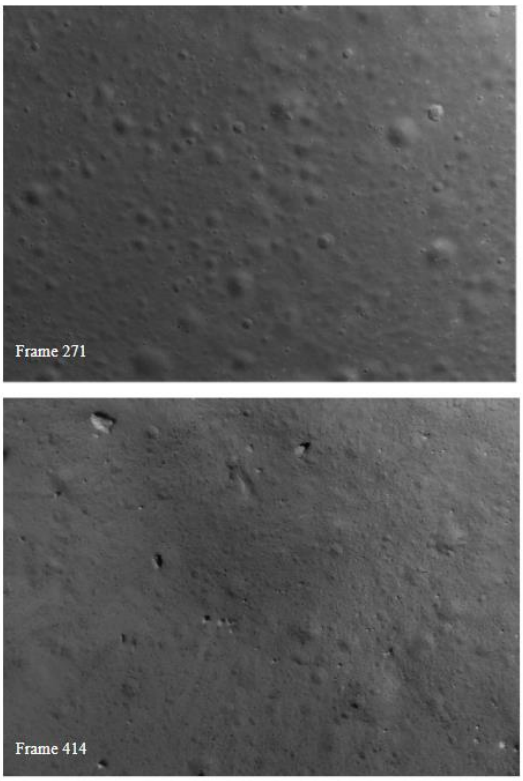

Figure 4. The first and the last frames of the selected series of the descent images.

Parameter	Value	unit
Pixel size	7.4	μm
Width	2352	pixel
Height	1728	pixel
Focal length	15.4	mm
Principle point_x0	1164.02	pixel
Principle point_y0	858.04	pixel

Table 1. Intrinsic and internal orientation parameters of the CE-5 descent camera.

Based on these selected images, a free model was generated using the software ContextCapture (Bentley, 2022) and 21 source 3D key points corresponding to the reference 3D key points in Figure 2 (a) were remained after outlier removal (as shown in Figure 5).

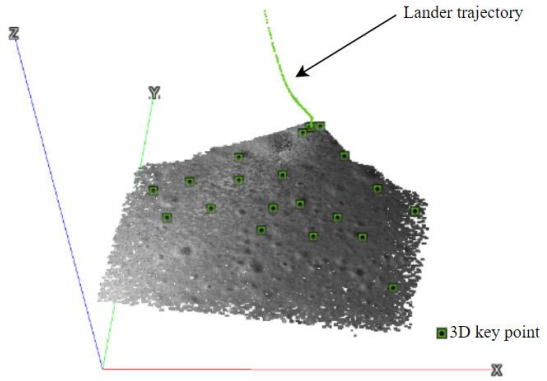

Figure 5. Free model generated from the selected CE-5 descent images.

3.1.2 Reference Data: The reference data include a DEM product generated from CE-2 stereo images (CE2TMap2015, DOI: http://www.dx.doi.org/10.12350/CLPDS.GRAS.CE2.DEM-20m.vA), and a geo-referenced LROC NAC image M1361560086RE. The resolution of CE2TMap2015 is 20 m/pixel and also can be downloaded from the China's Lunar and Planetary Data Release System. The LROC NAC image has a resolution of 1.19 m/pixel and is downloaded from PDS Geosciences Node Lunar Orbital Data Explorer (https://ode.rsl.wustl.edu/moon/index.aspx). Based on the CE-5 lander localization result (Wang et al., 2021), a rough range of the covering area of the CE-5 descent images was defined and the reference data in this area are shown in Figure 6.

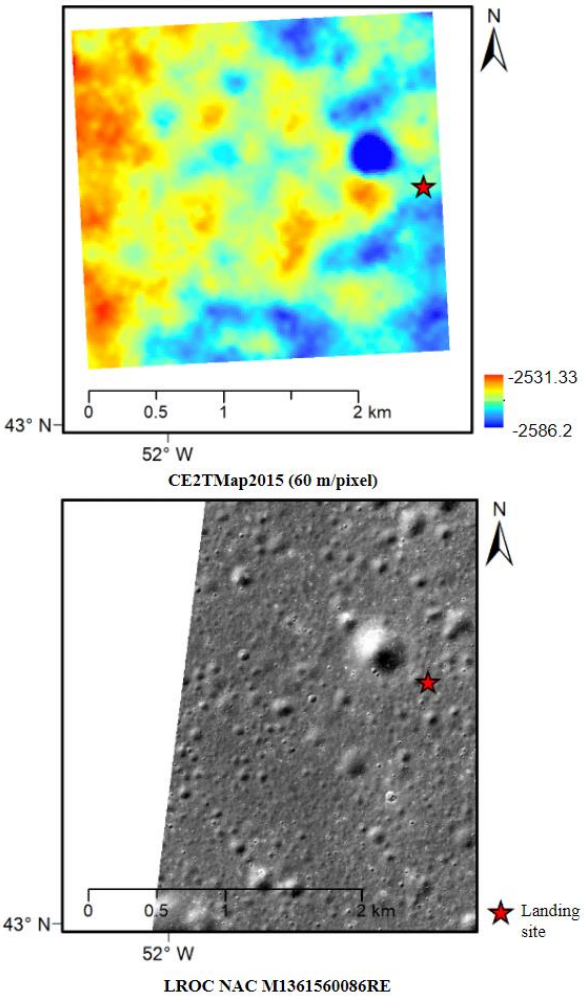

Figure 6. Reference data used for 3D geo-referencing.

3.2 3D Geo-referencing Result and Evaluation

Based on Equation (11), all the source 3D key points were transformed together with $\boldsymbol{m}$ into the geo-referenced model $\boldsymbol{M}$ (To solve the problems in Equation (2) and (4), open-source libraries Eigen (https://eigen.tuxfamily.org/) and Ceres Solver (http://ceres-solver.org/) were used). The differences between the 3D key points in $\boldsymbol{M}$ and the referenced 3D key points are shown in Table 2, where D_{XY} and D_Z are the horizontal and vertical distances between the 3D key points in $\boldsymbol{M}$ and those in the reference data.

In addition, we also conducted two contrast experiments. The direct 3D alignment computed the 3D rotation matrix, translation and scale factors between two sets of 3D points as in Equation (12).

$$\boldsymbol{P} = s \cdot R \cdot \boldsymbol{p} + \boldsymbol{T}, \tag{12}$$

And the GCPs method directly used the reference 3D key points as GCPs for bundle adjustment as in Di et al. (2020) and Liu et al. (2019).

Point ID	*3D-2D alignment*		*Direct 3D alignment*		*GCPs (ContextCapture)*	
	D_{XY}	D_Z	D_{XY}	D_Z	D_{XY}	D_Z
0	0.719	7.334	0.808	8.414	1.136	1.392
1	3.125	1.944	4.058	0.390	0.412	0.023
2	3.112	2.603	4.039	0.170	0.502	0.165
3	1.826	0.430	2.393	0.009	0.418	0.022
4	1.229	2.839	1.334	0.328	1.497	0.103
5	2.588	1.930	3.597	1.650	2.331	2.380
6	3.635	0.896	4.474	1.050	0.614	0.317
7	0.940	2.924	3.274	14.151	3.984	10.060
7	1.087	5.379	1.475	1.232	1.876	0.874
8	2.020	2.273	2.324	0.088	1.024	0.302
10	4.772	7.769	7.864	17.653	13.175	20.932
11	2.000	2.472	1.491	1.033	0.812	1.128
12	1.614	3.066	1.280	2.633	1.717	0.357
13	0.811	1.788	1.231	1.414	0.663	0.846
14	2.355	1.068	3.122	2.389	1.028	1.902
15	5.322	4.037	5.403	8.995	1.211	1.375
16	1.217	1.088	0.797	0.733	0.945	2.525
17	2.728	3.331	2.838	0.224	1.213	0.227
18	0.120	0.661	0.510	2.372	0.812	3.051
19	0.193	3.184	0.413	5.470	1.695	8.663
20	4.482	3.770	4.917	7.516	7.986	10.738
Mean	2.185	2.895	2.745	3.710	2.145	3.208
St. Dev.	1.475	1.967	1.916	4.942	3.029	5.222

Table 2. Evaluation of the 3D geo-referencing

From Table 2 it can be seen that both our method and the GCPs method than better result than the direct 3D alignment. While our results have comparable mean values of the horizontal and vertical differences with the GCPs method, the stand deviations of our results were much lower than the GCPs method, indicating more equilibria in our result. In fact, the reason of the GCPs method having a fairly good result is that the reference 3D key points were all laid at flat ground and the effects of the vertical inaccuracies in the reference CE2TMap2015 were greatly reduced while there being no terrain reliefs. It can be imagined that if the reference 3D key points are laid at an oblique plane, errors in the results of the GCPs method will be greater.

3.3 Evaluation of the CE-5 Descent Image DEM and DOM

With the geo-referenced model $\boldsymbol{M}$, high-resolution DEM and DOM products were generated from the CE-5 landing site. As the GSP of the descent image varies while the lander descending, we generated DEM/DOM covering different areas with different resolutions.

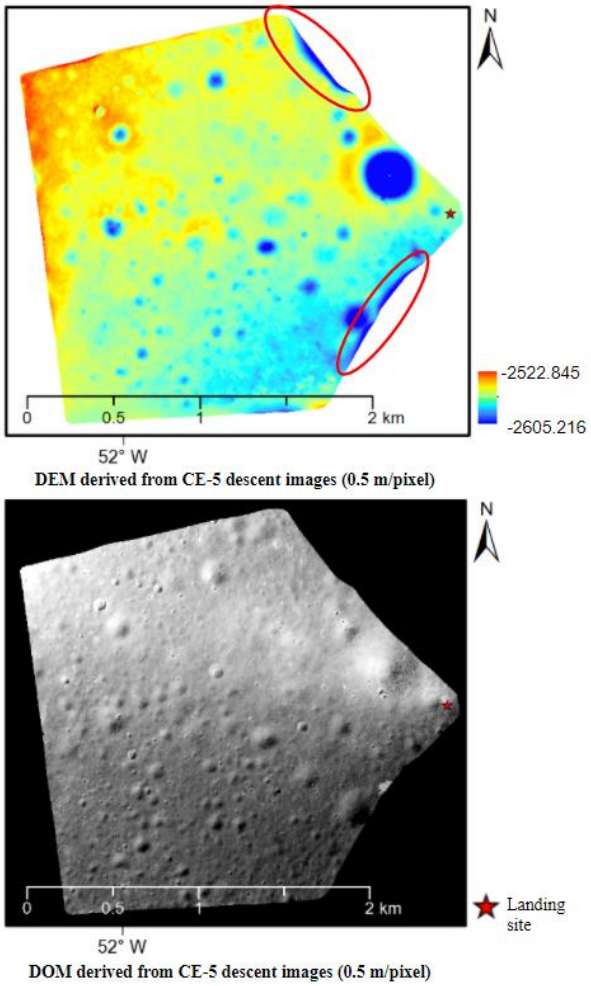

Figure 7. DEM and DOM (0.5 m/pixel) covering the entire area.

Figure 7 shows the DEM and DOM with a resolution of 0.5 m/pixel of the CE-5 landing site area covered by all of the selected descent images. To comprehensively evaluate the precisions of the generated DEM, we calculated the pixel-wise difference between the CE-5 DEM and the CE2TMap2015 and the result is shown in Figure 8. According to this pixel-size evaluation, the average absolute difference between the CE-5 DEM and the CE2TMap2015 is 2.78 m. Generally, the absolute difference is smaller than 5 m for flat areas, and most large differences appear at crater areas, especially large craters. But it is notable that CE-5 DEM is prone to having lower qualities at the edge of the covering area (as shown in the red ellipses in Figure 7), this may because the descent images have less overlapping at these edge areas, leading to bad aero-triangulation result during the generation of the free model, and consequently is reflected in the generated DEM.

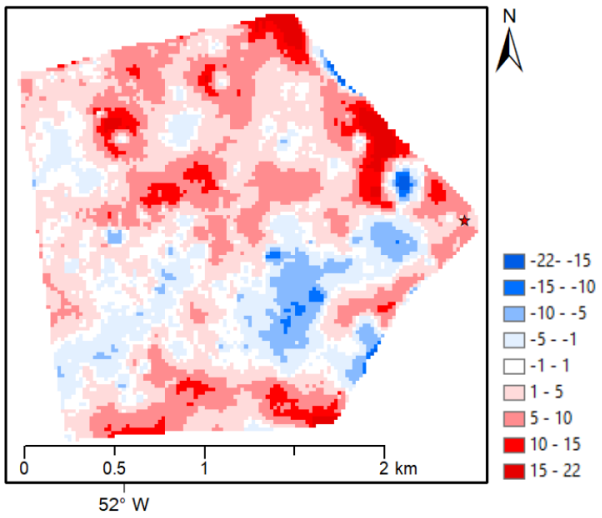

Figure 8. Height difference between distribution map (20 m/pixel) between the CE-5 DEM and the CE2TMap2015. The red means the CE-5 DEM has a greater value than the CE2TMap 2015, and blue means a less value.

Compared to the reference data, the high-resolution DEM and DOM enable identifying more fine-scale geographic features, e.g. small craters and rocks, as shown in Figure 9. DEM and DOM with a much higher resolution (0.01 m/pixel) were also generated for the CE-5 landing site as shown in Figure 10. These products allow extracting rocks and craters at centimetre to decimetre scale and will facilitate nearly in-situ studies with more in-depth findings.

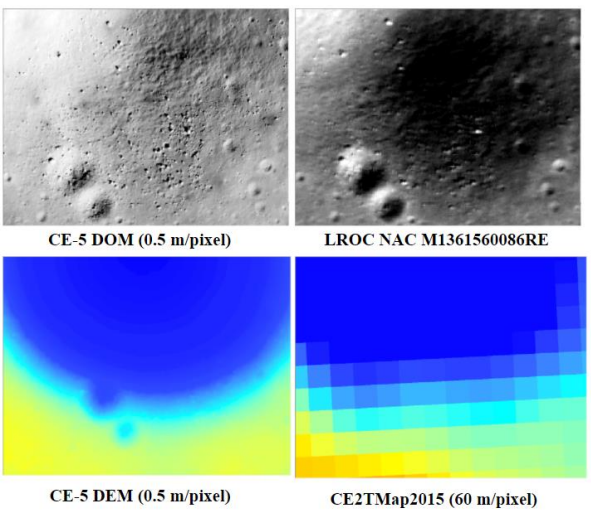

Figure 9. Comparison between the CE-5 DEM/DOM and the reference data in a local area.

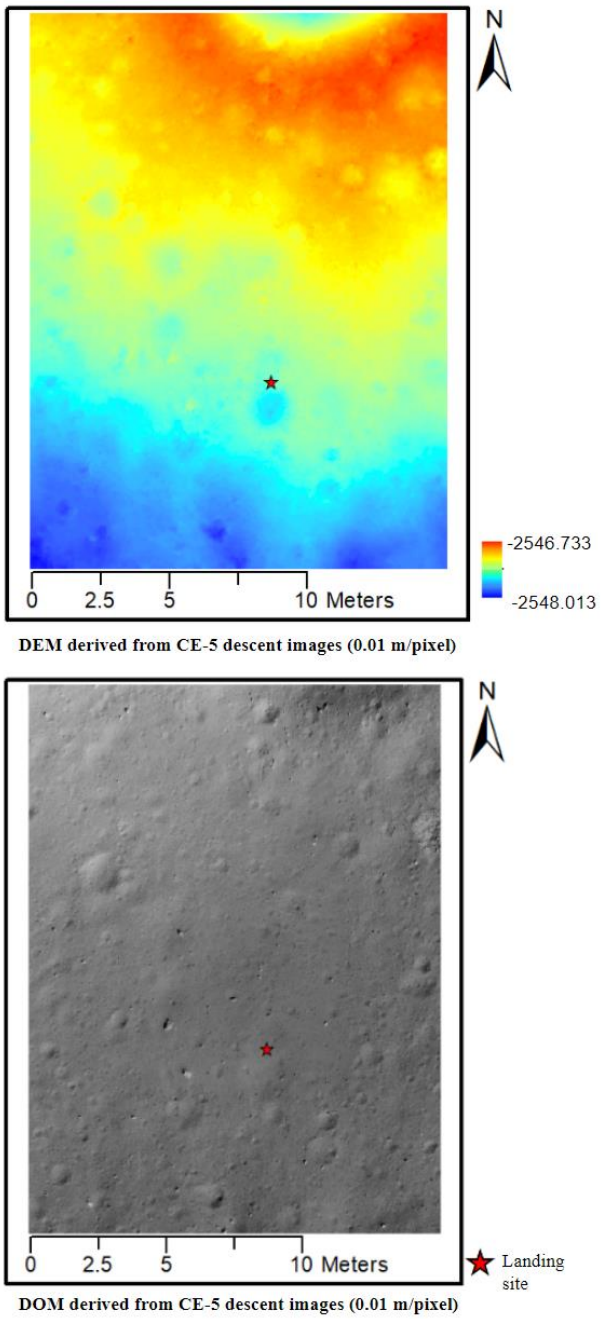

Figure 10. DEM and DOM (0.01 m/pixel) covering the CE-5 landing site.

4. CONCLUSIONS AND DISCUSSION

In regard to the common unevenness of accuracies in vertical and horizontal directions in the reference data for planetary data geo-referencing, this paper proposes a novel method that leverages the separated 3D and 2D alignments to control the distribution of geo-referencing errors. Compared to the traditional GCPs method, the proposed method had a more equilibrated error adjustment result.

Based on the geo-referenced model, high-resolution DEM and DOM products were generated for the CE-5 landing site. These product present much more features and details with resolutions at centimetre to decimetre scale, and therefore are able to support more in-depth scientific studies from micro perspectives.

ACKNOWLEDGEMENTS

This work was funded by the National Natural Science Foundation of China (Nos. 42201476) and the Open Fund of State Key Laboratory of Remote Sensing Science (OFSLRSS 202108).

REFERENCES

Barker, M.K., Mazarico, E., Neumann, G.A., et al., 2016. A new lunar digital elevation model from the Lunar Orbiter Laser Altimeter and SELENE Terrain Camer. *Icarus*, 273: 346-355.

Bentley, 2022. ContextCapture Software, Version 4.4.14.60. bentley.com/en/products/brands/contextcapture.

Besl, P.J., McKay, N.D., 1992. Method for registration of 3-D shapes. *Sensor fusion IV: control paradigms and data structures. International Society for Optics and Photonics*, 1611: 586-606.

Björck, A., 1990. Least squares methods. *Handbook of numerical analysis*, 1990, 1: 465-652.

Di, K., Liu, Z., Wan, W., et al., 2020. Geospatial technologies for Chang'e-3 and Chang'e-4 lunar rover missions. *Geo-spatial Information Science*, 23(1): 87-97.

Guo, D., Fa, W., Wu, B., Li, Y., Liu, Y., 2021. Millimeter‐to Decimeter‐Scale Surface Roughness of the Moon at the Chang'e‐4 Exploration Region. *Geophysical Research Letters*, 48(19): e2021GL094931.

Li, C., Liu, J., Ren, X., et al., 2018. Lunar global high-precision terrain reconstruction based on Chang'E-2 stereo images. *Geomatics and Information Science of Wuhan Unviersity*, 43: 486-495.

Linder, W., 2013. *Digital photogrammetry: theory and applications*. Springer Science & Business Media, 2013.

Liu, J., Ren, X., Yan, W., et al., 2019. Descent trajectory reconstruction and landing site positioning of Chang'E-4 on the lunar farside. *Nature communications*, 10(1): 1-10.

Schnabel, R., Wahl, R., Klein, R., 2007. Efficient RANSAC for point‐cloud shape detection. *Computer graphics forum. Oxford, UK: Blackwell Publishing Ltd*, 26(2): 214-226.

Wang, J., Zhang, Y., Di, K., et al., 2021. Localization of the Chang'e-5 Lander Using Radio-Tracking and Image-Based Methods. *Remote Sensing*, 13(4): 590.

Wang, Y., 2012. Gauss–newton method. *Wiley Interdisciplinary Reviews: Computational Statistics*, 4(4): 415-420.

Wu, B., Li, Y., Liu, W.C., et al., 2021. Centimeter-resolution topographic modeling and fine-scale analysis of craters and rocks at the Chang'E-4 landing site. *Earth and Planetary Science Letters*, 553: 116666.

APPENDIX

The original coordinates of the reference and source 3D key points are provided here.

Point ID	*Reference 3D key points*		
	X	*Y*	*Z*
0	-3238.264	1305159.012	-2541.928
1	-2038.602	1305678.998	-2550.104
2	-2051.063	1305697.016	-2549.326
3	-2150.296	1305734.018	-2551.140
4	-2991.857	1306030.890	-2544.194
5	-3922.198	1304589.858	-2550.290
6	-2016.602	1305619.606	-2553.405
7	-3143.731	1305480.950	-2546.438
7	-2665.528	1306135.210	-2554.093
8	-3121.520	1306391.850	-2543.056
10	-2991.821	1304606.068	-2558.991
11	-3556.629	1305660.567	-2543.613
12	-3405.485	1306111.259	-2548.391
13	-3422.948	1304921.769	-2547.414
14	-3610.987	1306389.019	-2544.876
15	-2774.744	1304953.528	-2548.111
16	-3519.283	1305272.418	-2546.542
17	-2395.984	1305312.879	-2555.634
18	-2820.702	1305715.090	-2548.080
19	-3269.234	1305658.945	-2550.368
20	-3320.041	1306620.318	-2547.418

Point ID	*Source 3D key points*		
	x	*y*	*z*
0	2.834	-8.444	-3.976
1	0.693	3.965	-6.083
2	0.493	3.888	-6.061
3	-0.075	3.051	-5.915
4	-4.833	-4.077	-4.462
5	6.617	-16.191	-2.710
6	1.303	4.034	-6.139
7	0.005	-6.786	-4.286
7	-5.055	-0.793	-5.139
8	-8.546	-4.414	-4.282
10	8.620	-7.514	-4.216
11	-2.685	-10.208	-3.451
12	-6.589	-7.727	-3.784
13	4.644	-10.732	-3.612
14	-9.695	-8.965	-3.492
15	5.912	-4.608	-4.804
16	1.083	-10.786	-3.484
17	3.374	-0.221	-5.483
18	-1.455	-3.231	-4.720
19	-1.978	-7.541	-3.941
20	-11.149	-5.720	-3.946